Lifetime and Performance Prediction of SOFC Anodes Operated with Trace Amounts of Hydrogen Sulfide

M. Riegraf[a], G. Schiller[a], R. Costa[a], K. A. Friedrich[a], A. Latz[a,b], V. Yurkiv[a]

[a] German Aerospace Centre (DLR), Institute of Engineering Thermodynamics, 70569 Stuttgart, Germany
[b] Helmholtz Institute Ulm (HIU), Electrochemical Energy Storage, 89081 Ulm, Germany

An elementary kinetic model is developed to predict the influence of sulfur on Ni/YSZ anodes of solid oxide fuel cells (SOFC) performance. A multi-step reaction mechanism describing the formation and oxidation of sulfur on the Ni surface is coupled with gas transport in the channel and porous phase, and charge-transfer processes. A thermodynamic and kinetic data set of sulfur formation and oxidation is derived based upon various literature sources including a coverage-dependent description of the enthalpy of surface-adsorbed sulfur. The validity of the model is demonstrated on two SOFC operation modes, namely $H_2/H_2O/H_2S$ and $CH_4/H_2/H_2O/H_2S$ fuel mixtures, at different operating conditions using various electrochemical literature experiments. The first concern is the influence of adsorbed sulfur on charge-transfer processes and the second concern is the effect of adsorbed sulfur on complex methane reforming chemistry. The results reveal that sulfur surface coverage increases with current density demonstrating a low sulfur oxidation rate.

Introduction

The massive usage of fossil fuels over the last decades has led to a large release of green-house gases impacting the climate. This has increased the needs to develop alternative energy conversion technologies with a reduced carbon-footprint. In this regard, Solid Oxide Fuel Cell (SOFC) is a promising alternative technology for energy supply (1). Being a high-temperature electrochemical device, SOFC can easily be operated on natural gas and a variety of hydrocarbons (e.g. methane, propane, dodecane) with a higher efficiency than conventional thermal power stations (2). An alternative and very promising source of hydrocarbons is biomass gasification. The obtained biogas (mainly methane and carbon oxides) is a renewable fuel source which can contribute to the reduction of fossil fuel usage and emission of greenhouse gases. However, depending on the content of biomass, the resulting biogas may contain some undesirable species that upon contact with the SOFC anode could lead to electrode degradation. One of such compounds is hydrogen sulfide, which via catalytic dissociation at the anode surface is converted into atomic hydrogen and sulfur. Therefore, understanding the origin and evolution of sulfur poisoning degradation processes, which typically take place on micro- and nanoscales, is essential in order to develop a long-term-operating SOFC technology.

Many studies have experimentally investigated the dependency of sulfur poisoning in Ni/YSZ anodes (3–9) on a wide range of operating conditions, such as temperature, current density, gas phase composition and operation modes. In all experimental studies, independent of the employed fuel gas mixture, a rapid initial power output drop occurs already for H_2S concentrations in the ppm range and is accompanied by a large increase in total anode

resistance (5,6). This drop is generally believed to be the result of the chemisorption of sulfur on the active surface sites, resulting in a blockage of the hydrogen oxidation reactions. The removal of H_2S from the gas feed usually leads to a full recovery of the electrocatalytic properties of the surface after short-time exposure (8–10).

Recently, in an attempt to explore SOFC operation in more advanced fuels, several studies have been conducted to investigate sulfur poisoning of SOFC run on methane-containing gases. These studies have indicated that the methane steam reforming reaction process is poisoned to an even larger extent than the electrochemical oxidation of hydrogen (10–13).

This study presents a modeling work of SOFC operated on H_2/H_2O and $CH_4/H_2/H_2O$ gas mixtures with different concentrations of H_2S in order to allow for a deeper understanding of the processes leading to sulfur poisoning. The developed model is validated against various experimental data from literature. The model couples a detailed multi-step reaction mechanism of sulfur formation and oxidation at Ni/YSZ anodes, complex reforming chemistry with supply channel gas-flow, porous-media transport and elementary charge-transfer chemistry.

Physical and Chemical Models

Physical Model

The simulation approach together with mathematical model is documented in our previous work (14,15) and only a brief summary is presented here. All chemical processes (chemical and electrochemical) are formulated as elementary reactions. The rate of all processes is described by mass-action kinetics under the mean-field assumption (16). Composite electrodes are represented in a continuum approach using effective transport coefficients for mass and charge. The gas transport within the porous phase is described by Stefan-Maxwell and Darcy viscous flow. The model is one-dimensional throughout the thickness of electrodes and electrolyte. Two SOFC configurations are used in the present study, i.e. button and planar setup design. The gas supply volume in the button cell design is represented by an isothermal finite-gap stagnation point flow model using a one-dimensional representation of the Navier-Stokes equations (17). In the case of a planar cell the transport of the gaseous reactants and products to and from the surface, respectively, takes place through convection and diffusion in the channel parallel to the electrode surface, described by a 1D representation of the Navier-Stokes equations (18). Current-voltage relationships are modeled by directly solving for the electric-potential distribution in the electrodes and electrolyte taking into account the electrical double layer capacitance.

Reaction Mechanism: Heterogeneous Chemistry on Ni and Charge-Transfer

A thermodynamic and kinetic data set for the respective reaction species and elementary reactions was derived and thoroughly described in our previous work in order to obtain a physically meaningful description of sulfur poisoning (19). It consists of hydrogen sulfide adsorption and dissociation on Ni surface with consecutive sulfur oxidation. All thermodynamic and kinetic data were derived based on literature available DFT calculations and chemical reactor experiments. Regarding the thermodynamic data of nickel-adsorbed sulfur, we assume a coverage-dependent enthalpy, which was derived based on H_2S adsorption isotherms for a variety of conditions (19). This data was then used to extend already existing reaction mechanisms for the respective gas phase compositions. For the H_2/H_2O system, a previously developed and validated reaction mechanism of H_2 oxidation at Ni/YSZ SOFC anodes was used as a basis (20,21). For the $CH_4/H_2O/H_2$ system, the full

mechanism of methane reforming on nickel, previously developed by Deutschmann and co-workers, was used (22,23). The reaction mechanism consists of 42 surface reactions among 6 gas phase species and 14 surface adsorbed species. All kinetic and thermodynamic data is used from the mentioned paper without any changes. In this study, the charge-transfer reaction is described by hydrogen spillover that transfers a proton from the Ni to a hydroxyl ion on the YSZ forming water and delivering one electron to the Ni. The respective rate coefficients (pre-exponential factor and activation energy) are taken from the previously validated reaction mechanism (24).

Model Parameterization

We use the model described above to analyze two sets of electrochemical experiments of SOFC running on (*i*) $H_2/H_2O/H_2S$ fuel and (*ii*) $CH_4/H_2O/H_2/H_2S$ fuel. In the first fuel mixture, the experimental results of Yang et al. (8) and Zha et al. (4) were used. In both of these studies a button-cell configuration was employed. Yang et al. have characterized anode-supported cells, whereas Zha et al. have examined electrolyte-supported SOFC. In the second hydrocarbon-containing fuel mixture, electrochemical measurements by Rasmussen et al. (10) were used who investigated the influence of H_2S on Ni/YSZ-based anode-supported planar SOFC. Both experimental measurements cover an extended range of operating temperatures ($1023\ K \leq T \leq 1123\ K$) and various gas compositions. The detailed geometrical parameters and the employed gas phase compositions are described in the respective references.

Simulation Procedure

Simulations were carried out using the in-house software package DENIS. All model equations used in the present paper are thoroughly described elsewhere (14). Spatial derivatives of the PDE system are discretized by the finite volume method and the resulting differential algebraic equation (DAE) system is integrated by means of the semi-implicit extrapolation solver LIMEX (25). Experimental electrochemical impedance spectra were simulated using a potential step and current relaxation technique (26). The impedance is obtained in the frequency domain of interest (10^{-3} to 10^6 Hz) by a Fourier transformation of the resulting time-domain traces of current and potential. For transient calculations, the solution (potential or current density) is determined at each time step by solving the transient system. Then the appropriate current density is obtained for a given overpotential.

Results and Discussion

First, we analyze simulation results for the simple H_2/H_2O gas system, where experiments by Yang et al. (8) and Zha et al. (4) are used (first subsection) and, second, experiments by Rasmussen et al. (10) for the gaseous $CH_4/H_2O/H_2$ system are used to explore the influence of sulfur on cell performance and on reforming chemistry particularly (second subsection).

Degradation of SOFC Operating on H_2/H_2O Gaseous System

Yang et al. have investigated anode-supported cells with a Ni-YSZ anode, LSCF cathode and a base anode fuel mixture of 50% H_2/1.5% H_2O/48.5% N_2. Fig. 1 shows the comparison between experimental and simulated electrochemical impedance spectra for systems before and after exposure to 1 ppm H_2S at various current densities and T = 1023 K. The experimental results have shown the trend of a smaller relative increase in cell resistance for higher current densities. Since the simulated Nyquist plots (left panel) are in very good

agreement with the experimental results, it can be concluded that our model is able to reproduce this characteristic poisoning behavior.

The influence of H_2S exposure on the system is also clearly demonstrated by the Bode plots in Figure 1 (right panel). It can be seen that at frequencies of about 10^1 Hz, where commonly surface processes take place (27,28), the presence of H_2S leads to a significant increase of the imaginary part of the impedance. Moreover, a small upwards shift of the initial Bode plot after the exposure to H_2S can be observed in the low frequency region between 10^{-3} and 10^{-1} Hz which corresponds to the gas concentration impedance.

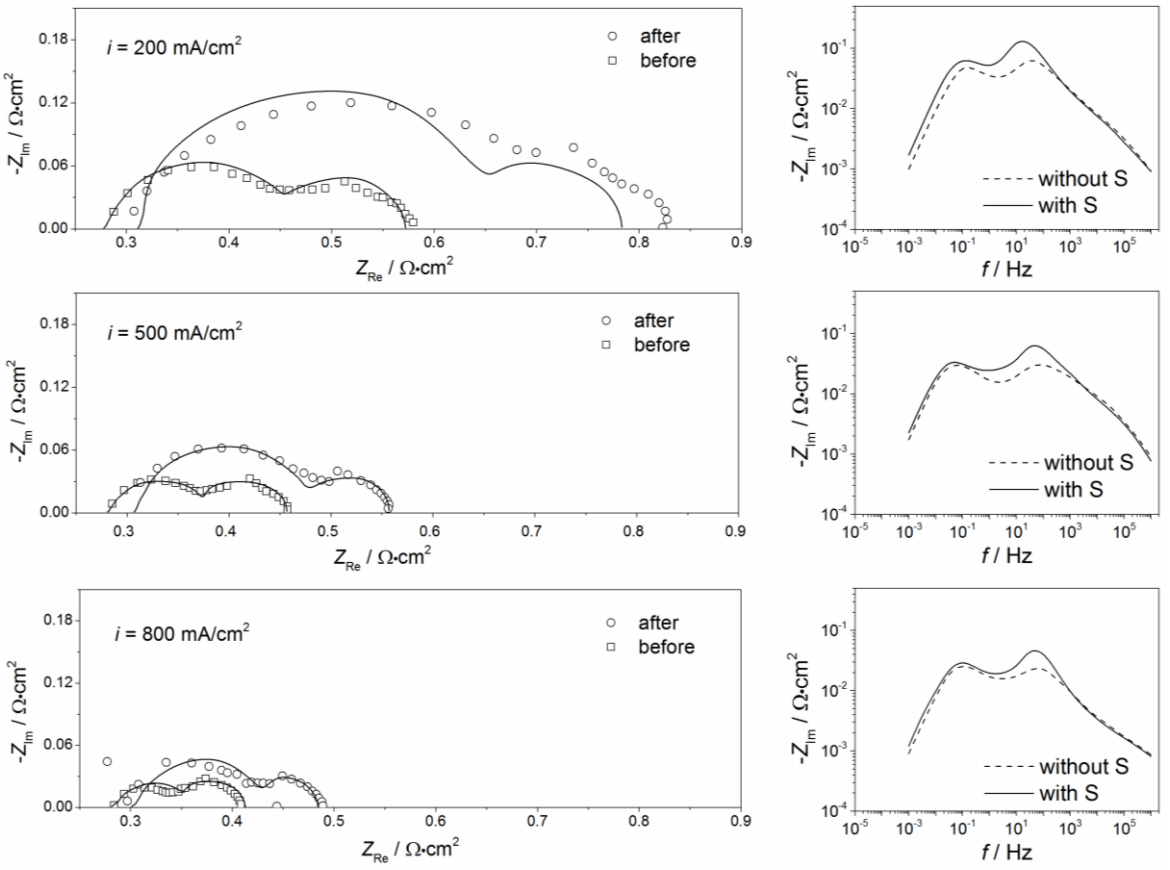

Figure 1. Nyquist (left panel) and Bode (right panel) plots of impedance spectra at a temperature of 1023 K and pressure of 1 atm before and after exposure to 1 ppm H_2S at various current densities. The experimental results are taken from Ref. (8). The left panel of the figure represents Nyquist plots of experiments and simulations. The right panel shows Bode plots of the imaginary part of the simulated complex impedance. There is no experimental data given for the Bode plots, thus, only simulation results are depicted.

Zha et al. have examined Ni/YSZ-based cells with LSM cathodes in a fuel mixture of 50% H_2/1.5% H_2O/48.5% N_2 with various trace amounts of H_2S at 1073 K. In Figure 2, the comparisons between the experimental and simulated results of the current density stability during the sulfur poisoning and recovery process are shown. In both cases the initial cell current density drop was successfully modeled by sulfur chemisorption at the nickel surface. Due to limited knowledge about the origins of the second-stage degradation for longer sulfur exposure times, it was modeled by a decrease in TPB length. The respective function was obtained via fitting. In the case of lower hydrogen sulfide concentration we obtained slower recovery, and for a concentration of 50 ppm the predicted recovery of the cell operation is

slightly faster, however, after a certain period of time the simulated and experimental current densities match well for both concentrations.

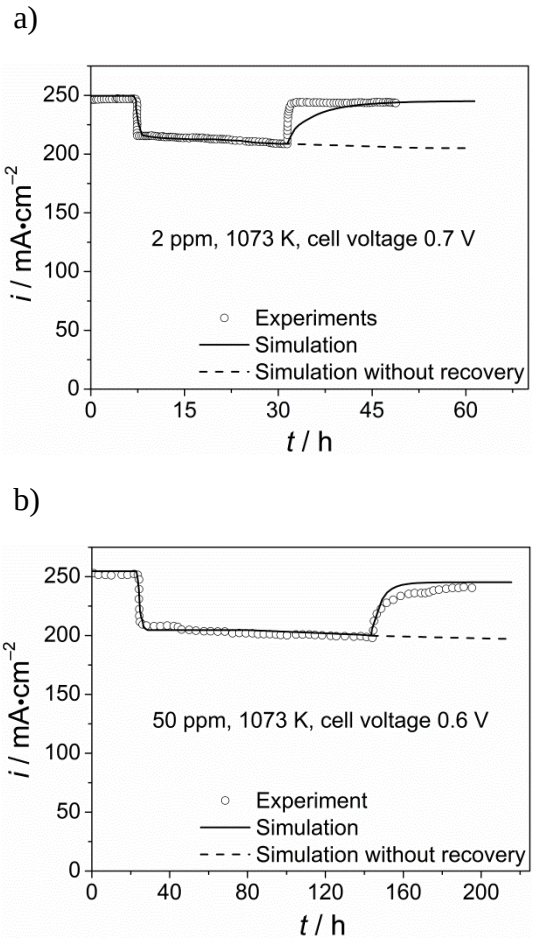

Figure 2. Simulated and experimental data for sulfur poisoning and regeneration processes of Ni-YSZ anodes in a fuel mixture with (a) 2 ppm (E = 0.7 V) and (b) 50 ppm H_2S (E = 0.6 V).

For deeper insights into the mechanistic details of sulfur poisoning, the calculated equilibrium sulfur coverage on the Ni surface as a function of current density is shown in Figure 3. It can be seen that at H_2S gas phase concentration of 50 ppm a considerably higher sulfur surface coverage is achieved than at 2 ppm. This can be assumed to be the reason for the higher current density drop at the 50 ppm system. The sulfur coverage for both 2 ppm and 50 ppm H_2S increases non-linearly with the current density. The reason for this behavior is likely to be the increase of the charge transfer reaction rate that results in a higher oxygen ion flux and enhanced H_2O water production. Therefore, more active surface sites become available for sulfur formation at higher current density. This is an interesting finding, since it is contrary to most previous studies, which have suggested the increase of the sulfur removal rate via electrochemical oxidation caused by the larger oxygen ion flux induced by high current densities (4,5,13,29,30).

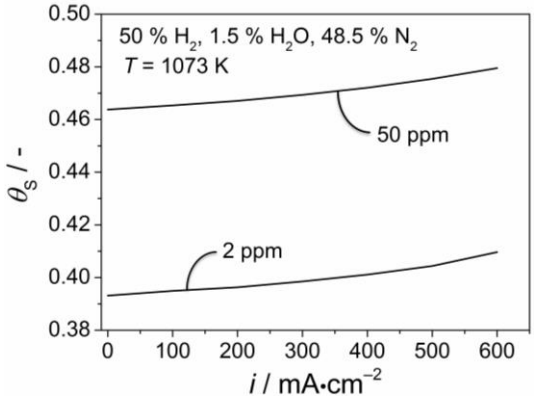

Figure 3. The change of sulfur coverage with cell current density for H_2S gas phase concentrations of 2 ppm and 50 ppm corresponding to results shown in Fig. 2ab.

Degradation of SOFC Operating on $CH_4/H_2/H_2O$ gaseous system

In this section the comparison between our simulations and the experiments by Rasmussen et al. (10) for a temperature of 1123 K at OCV is shown. As adsorbed elemental sulfur blocks the surface and thus, reduces the active Ni area, we describe this reduction with a simple exponential function as follows $A_{\mathrm{Ni}}^{\mathrm{V}} = A_{\mathrm{Ni},0}^{\mathrm{V}} \cdot e^{-9\cdot\theta(\mathrm{S_{Ni}})}$, where $A_{\mathrm{Ni}}^{\mathrm{V}}$ denotes the volume-specific surface area, $A_{\mathrm{Ni},0}^{\mathrm{V}}$ describes the initial volume-specific surface area and $\theta(\mathrm{S_{Ni}})$ is the sulfur coverage on the Ni surface.

Firstly, the OCV stability tests over 270 hours are reproduced in which the model is run with time-varying inputs monitoring different electrochemical performance changes. Figure 4 shows the results of the transient simulations for a 13 % H_2, 29 % CH_4, 58 % H_2O gas mixture and 2, 4, 7, 9, 20 and 24 ppm of hydrogen sulfide. At the beginning, up to 6 hours, the OCV has a constant value of 0.995 V, since no H_2S was introduced to the system. However, starting from 7 hours, the OCV gradually decreases over 43 hours upon operation with a constant H_2S concentration of 2 ppm. The increase of H_2S concentration initially leads to a further decrease of voltage, however, a stabilization of the cell voltage occurs for the H_2S concentrations higher than 20 ppm. Moreover, it can be observed that the initial decrease of cell voltage for 2 ppm H_2S proceeds at a much lower rate than the consecutive drops. A removal of H_2S from the feed gas results in a nearly complete voltage recovery.

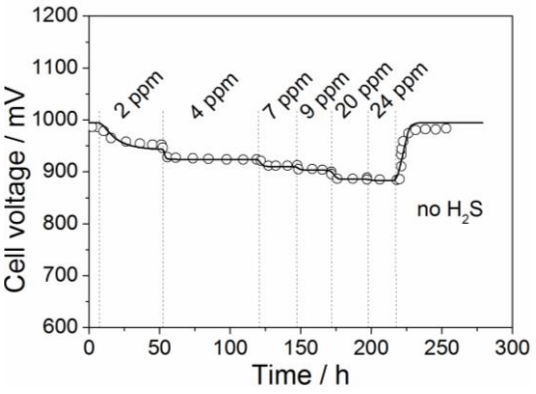

Figure 4. Comparison of the cell voltage (OCV) development at different H_2S concentrations between simulation (solid line) and experiments (open symbols) at T = 1123 K for 13 % H_2, 29 % CH_4, 58 % H_2O.

In order to allow for an in-depth analysis of the results shown in Fig. 4, the evolution of the main adsorbates' coverage on the nickel surface over 270 hours is shown in Fig. 5. It can be seen that the initial addition of 2 ppm H_2S leads to a significant increase in sulfur coverage and a simultaneous reduction of hydrogen and CO coverage. Subsequently, with a further increase in H_2S concentration, the sulfur surface coverage approaches its saturation coverage of 0.5 ML (31) and the values of hydrogen and CO coverage stabilize. The comparatively slow rate of this initial poisoning process is likely to be due to the only gradual replacement of the original surface adsorbates. This takes a particularly long time, as the initial poisoning entails by far the largest increase in sulfur coverage.

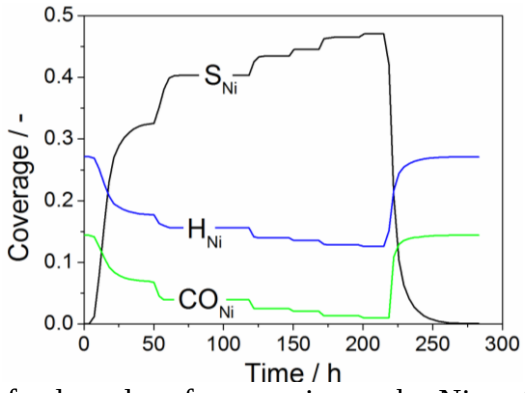

Figure 5. The coverages of selected surface species at the Ni surface during cell poisoning with 2, 4, 7, 9, 20 and 24 ppm of H_2S. Experimental conditions are the same as for the results in Fig. 4.

Finally, one example at constant current density of 1 $A \cdot cm^{-2}$ serves to demonstrate the capabilities of the model under polarization. Figure 6 illustrates the comparison between model prediction (line) and experimental measurements (open dots) for a gas mixture of 13 % H_2, 29 % CH_4, 58 % H_2O with 2 ppm H_2S concentration. The experimental conditions, used to model the results shown in Fig. 6, are the same as for OCV stability tests presented above. There are two distinguished regions in the results shown in Fig. 6. First, the cell operation in the absence of H_2S with the initial cell voltage of 688 mV, where constant overall slow cell degradation is observed, and the second region, where H_2S is introduced to the system causing a rapid voltage drop. There could be many reasons for this slow degradation in the absence of sulfur, however, in general most of these processes are associated with the decrease of TPB. Therefore, due to limited data available on the actual rate and type of these processes, we have modeled overall cell degradation via a continuous reduction of TPB length via the following equation $l^{V}_{Ni/YSZ} = l^{V}_{Ni/YSZ,0} \cdot e^{-\tau}$. In the second region, after about 450 h, when H_2S is introduced to the system, the cell voltage drops from 667 mV to 590 mV over 25 h. The cell performance drop in the presence of H_2S is reproduced taking into account complex reaction diffusion processes of sulfur formation/oxidation. As atomic sulfur is formed on the Ni surface, it diminishes the methane reforming rate causing a sudden voltage drop. This process is reversible as soon as constant H_2S supply is stopped.

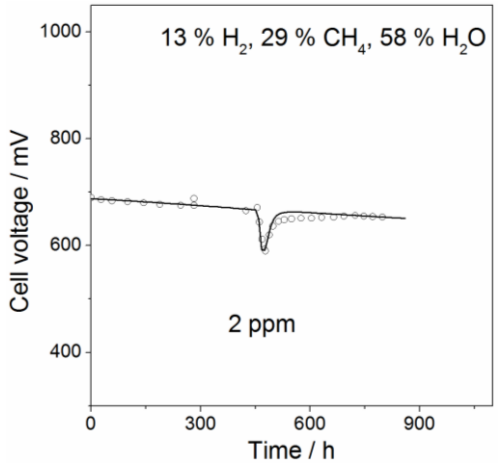

Figure 6. Comparison of cell voltage development for a constant current density of 1 A·cm^{-2} at 2 ppm H_2S concentration and T = 1123 K.

Summary and Conclusions

We have developed an elementary kinetic model of sulfur formation and oxidation on the Ni/YSZ anode of SOFC. The model was used to predict cell performance for a wide range of fuels and operating conditions. Literature taken impedance spectra, current density and voltage stability tests were successfully reproduced for different H_2S gas phase concentrations and temperatures.

The approach in this work consists of two steps. First, we have compared model predictions with the results of electrochemical experiments in the H_2/H_2O fuel system for a simple button cell design, and second, a model for the planar cell configuration is used to establish degradation rates and sulfur influence on cell performance.

Electrochemical results for the H_2/H_2O system show that at relatively low H_2S concentrations SOFC button-cell performance can be interpreted using chemical surface sulfur formation. However, when the H_2S concentration is sufficiently high, the inclusion of second stage degradation is necessary.

In the case of methane containing fuels, it was shown that the developed model, without any modifications, reproduces reasonably the observed voltages decrease, and is able to capture the changes in fuel conversion and selectivity for different gas mixtures. It was also shown that atomically adsorbed sulfur significantly influences the heterogeneous reforming chemistry, causing a significant degradation of the cell voltage. Consequently, it could be concluded that the addition of small amounts of hydrogen sulfide to methane significantly decreases fuel conversion and correspondingly carbon formation.

In addition to the above conclusions, the model also predicts the increase of sulfur surface coverage with current density for both systems.

Acknowledgments

We gratefully acknowledge financial support by the German Ministry of Education and Research via grant number 03SF0494C. V.Y. and R.C. acknowledge European Union's Seventh Framework Programme (FP7/2007-2013) for the Fuel Cells and Hydrogen Joint Technology Initiative under grant agreement n°303429.

References

1. S. C. Singhal and K. Kendall, in *High Temperature Solid Oxide Fuel Cells: Fundamental, Design and Applications, Elsevier Advanced Technology*, p. 410, Oxford, UK, (2003).
2. R. J. Kee, H. Zhu, a. M. Sukeshini, and G. S. Jackson, *Combust. Sci. Technol.*, **180**, 1207 (2008).
3. K. Sasaki et al., *J. Electrochem. Soc.*, **153**, A2023 (2006).
4. S. Zha, Z. Cheng, and M. Liu, *J. Electrochem. Soc. Soc.*, **154**, B201 (2007).
5. Z. Cheng, S. Zha, and M. Liu, *J. Power Sources*, **172**, 688 (2007).
6. Y. Matsuzaki and I. Yasuda, **132**, 261 (2000).
7. A. Lussier, S. Sofie, J. Dvorak, and Y. Idzerda, *Int. J. Hydrogen Energy*, **33**, 3945 (2008).
8. L. Yang, Z. Cheng, M. Liu, and L. Wilson, *Energy Environ. Sci.*, **3**, 1804 (2010).
9. J. F. B. Rasmussen and A. Hagen, *J. Power Sources*, **191**, 534 (2009).
10. J. F. B. Rasmussen and a. Hagen, *Fuel Cells*, **10**, 1135 (2010).
11. T. R. Smith, A. Wood, and V. I. Birss, *Appl. Catal. A Gen.*, **354**, 1 (2009).
12. A. Hagen, G. B. Johnson, and P. Hjalmarsson, *J. Power Sources*, **272**, 776 (2014).
13. J. R. Rostrup-Nielsen, J. B. Hansen, S. Helveg, N. Christiansen, and A. K. Jannasch, *Appl. Phys. A*, **85**, 427 (2006).
14. W. G. Bessler, S. Gewies, and M. Vogler, *Electrochim. Acta*, **53**, 1782 (2007).
15. V. Yurkiv, R. Costa, Z. Ilhan, A. Ansar, and W. G. Bessler, *J. Electrochem. Soc.*, **161**, F480 (2014).
16. S. B. Adler and W. Bessler, in *Handbook of Fuel Cells: Fundamentals, Technology and Applications*, Vol. 5, A. L. W. Vielstich, H. A. Gasteiger, and H. Yokokawa, Editors., p. 441, John Wiley & Sons Ltd., Chichester (2009).
17. W. G. Bessler, *J. Electrochem. Soc.*, **153**, A1492 (2006).
18. W. G. Bessler and S. Gewies, *J. Electrochem. Soc.*, **154**, B548 (2007).
19. M. Riegraf et al., *J. Electrochem. Soc.*, **162**, F65 (2015).
20. M. Vogler, A. Bieberle-Hütter, L. Gauckler, J. Warnatz, and W. G. Bessler, *J. Electrochem. Soc.*, **156**, B663 (2009).
21. W. G. Bessler et al., *Phys. Chem. Chem. Phys.*, **12**, 13888 (2010).
22. E. S. Hecht et al., *Appl. Cat. A Gen.*, **295**, 40 (2005).
23. L. Maier, B. Schädel, K. Herrera Delgado, S. Tischer, and O. Deutschmann, *Top. Catal.*, **54**, 845 (2011).
24. M. Vogler, A. Bieberle-Hütter, L. Gauckler, J. Warnatz, and W. G. Bessler, *J. Electrochem. Soc.*, **156**, B663 (2009).
25. P. Deuflhard, E. Hairer, and J. Zugck, *Numer. Math.*, **51**, 501 (1987).
26. W. G. Bessler, *J. Electrochem. Soc.*, **154**, B1186 (2007).
27. H. Zhu et al., *J. Electrochem. Soc.*, **159**, F255 (2012).
28. M. B. Mogensen et al., *Proc. EFCF 2014*, B1209 (2014).
29. E. Brightman, D. G. Ivey, D. J. L. Brett, and N. P. Brandon, *J. Power Sources*, **196**, 7182 (2011).
30. E. Brightman, R. Maher, D. Ivey, G. Offer, and N. Brandon, *ECS Trans.*, **35**(1), 1407 (2011).
31. J. Oudar, *Catal. Rev. Engmeering*, 37 (1980).